Chinese Journal of Natural Medicines

Salidroside inhibits osteoclast differentiation based on osteoblast-osteoclast interaction *via* HIF-1 α pathway

Yutong Jin, Yao Wang, Chuan Wang, Lingling Zhang, Dandan Gao, Haizhao Liu, Qingwen Cao, Chenchen Tian, Yuhong Bian, Yue Wang

Citation: Yutong Jin, Yao Wang, Chuan Wang, Lingling Zhang, Dandan Gao, Haizhao Liu, Qingwen Cao, Chenchen Tian, Yuhong Bian, Yue Wang, Salidroside inhibits osteoclast differentiation based on osteoblast-osteoclast interaction *via* HIF-1 α pathway, Chinese Journal of Natural Medicines, 2025, 23(5), 572-584. doi: 10.1016/S1875-5364(25)60864-8.

View online: https://doi.org/10.1016/S1875-5364(25)60864-8

Chinese Journal of Natural Medicines 23 (2025) 572-584

Contents lists available at ScienceDirect

Chinese Journal of Natural Medicines

journal homepage: www.cjnmcpu.com/

Original article

Salidroside inhibits osteoclast differentiation based on osteoblast-osteoclast interaction *via* HIF-1α pathway

Yutong Jin[a,b,Δ], Yao Wang[a,Δ], Chuan Wang[c,d,Δ], Lingling Zhang[a], Dandan Gao[a], Haizhao Liu[a], Qingwen Cao[a], Chenchen Tian[a], Yuhong Bian[a,b,*], Yue Wang[a,*]

[a] *School of Integrative Medicine, Tianjin University of Traditional Chinese Medicine, Tianjin 301617, China*
[b] *Department of Oncology, First Teaching Hospital of Tianjin University of Traditional Chinese Medicine, Tianjin 300193, China*
[c] *Department of Stomatology, NHC Key Laboratory of Hormones and Development, Chu Hsien- I Memorial Hospital and Tianjin Institute of Endocrinology, Tianjin Medical University, Tianjin 300134, China*
[d] *Department of Stomatology, Tianjin Key Laboratory of Metabolic Diseases, Tianjin Medical University, Tianjin 300134, China*

ARTICLE INFO

Article history:
Received 21 September 2024
Revised 25 October 2024
Accepted 2 January 2025
Available online 20 May 2025

Keywords:
Salidroside
Hypoxia-inducible factor-1α
Osteoblast
Osteoclast
Osteoclastogenesis

ABSTRACT

This study investigated the regulatory potential of salidroside (SAL), a primary active compound in *Rhodiola rosea* L., on osteoclast differentiation by modulating the hypoxia-inducible factor 1-alpha (HIF-1α) pathway in osteoblasts. Luciferase reporter assay and chromatin immunoprecipitation (ChIP) assay were employed to validate whether the receptor activator of nuclear factor-κB ligand (RANKL) is the downstream target gene of HIF-1α in osteoblasts. The study also utilized lipopolysaccharide (LPS)-induced mouse osteolysis to examine the impact of SAL on osteolysis *in vivo*. Furthermore, conditioned medium (CM) from SAL-pretreated osteoblasts was used to investigate the paracrine effects on osteoclastogenesis through the HIF-1α pathway. Hypoxic condition-induced overexpression of HIF-1α upregulated RANKL levels by binding to the RANKL promoter and enhancing transcription in osteoblastic cells. *In vivo*, SAL significantly alleviated bone tissue hypoxia and decreased the expression of HIF-1α by downregulating the expression of RANKL, vascular endothelial growth factor (VEGF), interleukin 6 (IL-6), and angiopoietin-like 4 (ANGPTL4). In the paracrine experiment, conditioned media from SAL-pretreated osteoblasts inhibited differentiation through the HIF-1α/RANKL, VEGF, IL-6, and ANGPTL4 pathways. RANKL emerges as the downstream target gene regulated by HIF-1α in osteoblasts. SAL significantly alleviates bone tissue hypoxia and bone loss in LPS-induced osteolysis through the HIF-1α/RANKL, VEGF, IL-6, and ANGPTL4 pathways. SAL inhibits osteoclast differentiation by regulating osteoblast paracrine secretion.

1. Introduction

Osteoporosis is a widespread skeletal disorder characterized by decreased bone mass and deterioration of bone tissue microarchitecture, leading to enhanced bone fragility and increased fracture risk [1]. This condition disproportionately affects the elderly population, particularly postmenopausal women. Among adults aged 40 years or older, the prevalence of osteoporosis is 5.0% in men and 20.6% in women [2]. Epidemiological data indicate that approximately 33% of older women and 20% of older men are at risk of osteoporotic fractures [3, 4]. While bisphosphonates are commonly prescribed for osteoporosis treatment, they are associated with potential adverse effects, including osteonecrosis and gastrointestinal complications [5, 6]. As a result, there is an increasing focus on identifying novel approaches for the prevention and treatment of osteoporosis.

The development of osteoporosis is closely associated with an imbalance between osteoblast-mediated bone formation and osteoclast-mediated bone resorption, with the latter being the primary contributing factor [7]. Both osteoblasts and osteoclasts are oxygen-sensing cells, and hypoxia has been linked to abnormal bone metabolism [8, 9]. A hypoxic microenvironment is a common characteristic of osteolytic diseases, including osteoporosis, playing a significant role in regulating bone remodeling and influencing disease prognosis and progression[10]. Hypoxia-inducible factor 1-alpha (HIF-1α), an oxygen concentration-dependent transcriptional regulatory factor, upregulates numerous genes under hypoxic conditions, including vascular endothelial growth factor (VEGF) [11]. Chronic intermittent hypoxia induces adaptive responses in the body or cells to maintain oxygen homeostasis. HIF-1α expression in both osteoblasts and osteoclasts can promote osteoclast differentiation and enhance bone resorption under specific hypoxic conditions [12].

Receptor activator of nuclear factor-κB ligand (RANKL), secreted by osteoblasts, plays a crucial role in osteoclast activation and differentiation. VEGF, strongly induced by HIF-1α, is a pro-angiogenic cytokine essential for angiogenesis. IL-6, a multifunctional cytokine, influences osteoclast differentiation. Angiopoietin-like 4 (ANGPTL4), a pro-angiogenic adipokine, en-

* Corresponding author.
E-mail addresses: bianyuhong_2012@163.com (Y. Bian); wangyue6808@126.com (Y. Wang)
Δ These authors contributed equally to this work.

https://doi.org/10.1016/S1875-5364(25)60864-8

hances osteoclast proliferation and differentiation. Previous studies have identified VEGF and ANGPTL4 as downstream target genes of HIF-1α [13, 14]. Additionally, our research group has demonstrated IL-6 as another downstream target gene of HIF-1α, implicating its involvement in bone resorption activity regulation [15]. The activation of HIF-1α and its downstream pathways, including VEGF, IL-6, and ANGPTL4, is critical in osteoclast regulation. Further research is necessary to comprehensively elucidate the mechanisms driving these effects and explore potential therapeutic strategies for osteoporosis treatment.

Traditional Chinese herbal medicines are attracting increased attention as potential treatments for osteoporosis due to their abundant resources, long-standing efficacy, and minimal side effects [16, 17]. Salidroside (SAL), the primary active compound in *Rhodiola rosea*, has been extensively studied for its anti-hypoxic and pro-angiogenic properties. Research has demonstrated that SAL mitigates hypoxia-induced osteoporosis by modulating cellular autophagy levels, oxidative stress response, and other pathways [18]. Our investigation revealed that conditioned medium (CM) from SAL-pretreated osteoblasts enhances the proliferation, migration, and capillary structure formation of endothelial cells, indicating that SAL promotes angiogenesis-osteogenesis coupling in endothelial cells by upregulating the HIF-1α/VEGF pathway in osteoblasts [19]. However, the potential influence of SAL on the HIF-1α pathway and its role in regulating osteoclast phenotypic expression through osteoblast paracrine secretion remains unexplored.

This study demonstrates that RANKL functions as a downstream target gene of HIF-1α in osteoblasts. SAL significantly mitigated bone tissue hypoxia and ameliorated bone loss in lipopolysaccharide (LPS)-induced osteolysis through HIF-1α/RANKL, VEGF, IL-6, and ANGPTL4 pathways. Furthermore, SAL inhibited the differentiation of co-cultured osteoclasts based on osteoblast-osteoclast interaction *via* these same pathways. These findings underscore the complex role of SAL in modulating osteoclastogenesis and the interplay between osteoblasts and osteoclasts.

2. Materials and methods

2.1. Materials

α-Minimum Eagle's medium (α-MEM) (SH30265.01), Dulbecco's modified Eagle medium (DMEM) (SH30021.01), fetal bovine serum (FBS) (SH30084.03), penicillin/streptomycin (Sv30010) were obtained from Hyclone, Logan, USA. Osteoclastogenesis -inducing factors macrophage colony stimulating factor (0815612) and RANKL (0817245) were acquired from PeproTech, NJ, USA. Lipofectamine™ 2000 was sourced from Invitrogen, CA, USA. SAL (S25475, $C_{14}H_{20}O_7$, ≥ 98%) was obtained from YUANYE Bio-Technology, Shanghai, China. $CoCl_2$ (232696, ≥ 97%) and YC-1 (Y102) were procured from Sigma, MO, USA. Avastin (H0201B05) was acquired from Roche, IN, USA. HIF-1α (ab1) and anti-IL-6 (ab9324) were obtained from Abcam, Cambridge, UK. Anti-β-actin (RM2001) was sourced from Ray Antibody Biotech, Beijing, China. MBL (DF4152), immunoglobulin G (IgG) (S0002) and immunohistochemistry (IHC) antibodies HIF-1α (BF8002), VEGF (AF5131), IL-6(DF6087), ANGPTL4 (DF6751) and RANKL(AF0313) were procured from Affinity Biosciences, Ohio, USA. Denosumab (CSD00157) was obtained from Chemstan Bio-Technology, Wuhan, China. Tartrate Resistant Acid Phosphatase (TRAP) kit (G1492), Methylthiazolyldiphenyl-tetrazolium (MTT) solution (M8180), Red Blood Cell Lysis (R1010), radio immunoprecipitation assay (RIPA) lysis buffer (R0010), Toluidine Blue O solution (G3663), 5% bovine serum albumin (BSA) (SW3015) and Annexin V-fluorescein isothiocyanate (FITC)/Propidium Iodide (PI) kit (CA1020) were acquired from Solarbio, Beijing, China. Hypoxyprobe-1 kit (HP2-100) was sourced from Hypoxyprobe Inc., MA, USA. TRIzol reagent (DP424) was obtained from Tiangen Biotech, Beijing, China. SYBR Green quantitative PCR (qPCR) SuperMix (AQ601-03) was procured from TransGen Biotech, Beijing, China. HiFiScript complementary deoxyribonucleic acid (cDNA) Synthesis Kit (CW2569M) and bicinchoninic acid (BCA) kit (CW0014S) were acquired from CWbio, Beijing, China. RANKL enzyme-linked immunosorbent assay (ELISA) kit (EK1208) was obtained from Multisciences Biotech, Shanghai, China. EasyBlot enhanced chemiluminescence (ECL) kit (WBKLS0100) was sourced from Millipore, MA, USA.

2.2. Extraction of primary osteoblasts and osteoclasts

2.2.1. Primary osteoblasts

Neonatal C57BL6 mice, less than 48 hours old, were placed in petri dishes within a super-clean bench environment. Their skulls were exposed by carefully removing the surrounding connective tissues using scissors. The skulls were then dissected into small fragments measuring approximately 1 mm × 1 mm. Subsequently, the tissues underwent digestion with 0.25% trypsin for 20 minutes, after which the digested liquid was discarded. Following this, 0.1% type I collagenase was applied for two digestion cycles, each lasting 1 hour. The resulting digested solution was collected and centrifuged. The cell precipitates were resuspended in α-MEM complete medium (containing 12% FBS, 1% penicillin/streptomycin). The medium was replaced the following day, and the identification of mouse primary osteoblasts (MOB) was performed after 1 week. The reagents and drugs utilized in this study are described in the supplementary materials.

2.2.2. Primary osteoclasts

The femur and tibia of 6-week-old C57BL/6 mice were isolated, and the bone marrow cavity was flushed with α-MEM medium (containing 1% penicillin/streptomycin). The resulting bone marrow suspension was centrifuged, and the supernatant was discarded. Subsequently, red blood cell lysis buffer was applied for 5 minutes, followed by another centrifugation step to remove the supernatant. The remaining cells were cultured in α-MEM complete medium (containing 12% FBS, 1% penicillin/streptomycin). After 24 hours, the culture supernatant was replaced with α-MEM complete medium supplemented with M-CSF (50 $ng \cdot mL^{-1}$), and RANKL (50 $ng \cdot mL^{-1}$). Mature osteoclasts derived from bone marrow macrophages (BMMs) were obtained after one week of culture.

2.3. Cell culture

To examine SAL's impact on HIF-1α transcriptional activity and RANKL expression regulation in osteoblasts, this study utilized human osteoblastic cell line MG-63, mouse osteoblastic cell line MC3T3-E1, and mouse preosteoclast cell line RAW264.7, all obtained from the American Type Culture Collection (ATCC, USA). Prior to co-culture experiments, RAW264.7 cells were differentiated into mature osteoclasts through treatment with M-CSF and RANKL. MG-63 and RAW264.7 were cultured in DMEM complete medium (containing 10% FBS, 1% penicillin/streptomycin), while MC3T3-E1, MOB, and BMMs were cultured in α-MEM complete medium (containing 12% FBS, 1% penicillin/streptomycin).

2.4. Cell transfection

To generate stable MG-63 cell clones with enhanced or inhibited endogenous HIF-1α expression, the plasmids [pCMVh-HA-ssHIF-1α, HIF-1α short hairpin ribonucleic acid (shRNA)], the

vector (pCMVh-HA) and scramble shRNA were utilized. MG-63 cells were transfected with these plasmids using Lipofectamine™ 2000. To examine the effect of HIF-1α on the transcriptional activity of RANKL in osteoblasts under hypoxia, MG-63 cells were transfected with the pGL3-hRANKL promoter-luc plasmid under hypoxic conditions. The pGL3-hRANKL promoter-luc plasmid was received as a gift from Dr. Sakamuri V. Reddy (Medical University of South Carolina, USA). This plasmid, along with pCMVh-HA or ssHIF-1α and SV40-β-galactosidase, was transfected into MG-63 cells at a ratio of 1 : 2 : 1 using Lipofectamine™ 2000. The transfected cells were utilized for subsequent tests within 24 h post-transfection.

2.5. Cell grouping and treatment

Cells were exposed to varying concentrations of SAL solutions (1, 10, 100, 1000 nmol·L^{-1}). The hypoxic groups were cultivated in a hypoxic incubator with 1% O_2 or treated with $CoCl_2$ (0.5 mmol·L^{-1}) for 24 h following 24 h of SAL treatment. In co-culture experiments, SAL was initially applied to the osteoblasts. The hypoxic conditions and duration of SAL action remained consistent with the aforementioned protocol. Subsequently, the culture supernatant was collected as CM to stimulate osteoclasts. In the blocking group, the following subgroups were added to the osteoblasts: HIF-1α specific blocking antibody YC-1 (10 μmol·L^{-1}) added 1 hour in advance; VEGF inhibitor Avastin (4 μg·mL^{-1}), Monoclonal anti-IL-6 antibody (0.3 μg·mL^{-1}), ANGPTL4 inhibitor MBL (10 μg·mL^{-1}), RANKL inhibitor Denosumab (10 μg·mL^{-1}), and IgG (control antibody) were added simultaneously with SAL. The combinative blocking (CB) group received a combination of YC-1, Avastin, anti-IL-6, MBL, and Denosumab.

2.6. Luciferase reporter assay

MG-63 cells were treated with SAL for 24 h, followed by exposure to one of three experimental conditions: standard incubator conditions, a hypoxic incubator with 1% O_2, or 0.5 mmol·L^{-1} $CoCl_2$ treatment for an additional 24 h. After treatment, cells were lysed to quantify luciferase activity using the Promega Luciferase Assay System. Luminescence measurements were obtained with a Fluoroskan Ascent™ FL Microplate Fluorometer and Luminometer (Thermo Fisher Scientific, Waltham, USA). In parallel, β-galactosidase activity was assessed using the ONPG substrate (Sigma) and measured at 420 nm with a BioTek ELX800 microplate reader (BioTek Instruments, France).

2.7. ChIP assay

MG-63 cells underwent lysis and sonication to obtain DNA fragments. After pre-clearance with blocked protein G agarose, the supernatant was immunoprecipitated by adding an HIF-1α antibody or an equivalent concentration of IgG. The mixture was incubated overnight at 4 °C. Following multiple washes, the protein was digested using proteinase K at 45 °C for 2 h to reverse the DNA-protein cross-linking. Subsequently, DNA was eluted from the immune complexes.

2.8. LPS-induced calvarial osteolysis model in mice

C57BL/6 mice (male, 6–8 weeks old) were acquired from Beijing Viton Lever Laboratory Animal Technology Ltd. (Beijing, China). To induce osteolysis with LPS, mice received intraperitoneal injections of LPS on days 2 and 5. The mice were randomly assigned to four groups: (1) control group (n = 8); (2) LPS group (n = 8) receiving LPS (5 mg·kg^{-1}) alone; (3) SAL-treated group (n = 8) receiving both LPS (5 mg·kg^{-1}) and SAL (5 mg·kg^{-1}); (4) SAL-treated group (n = 8) receiving LPS (5 mg·kg^{-1}) and SAL (20 mg·kg^{-1}). SAL was administered on day 1 and subsequently every other day. All mice were euthanized on day 8. Mice were labeled with the hypoxia probe (hypoxyprobe-1) *via* intraperitoneal injection 1 hour before euthanasia. The animal experiment was approved by the Experimental Animal Ethics Committee of Tianjin University of Traditional Chinese Medicine (Approval No.: TCM-LAEC2020130).

2.9. Micro-computed tomography (CT) scanning

The calvaria was immersed in a 4% paraformaldehyde solution for 48 h and subjected to micro-CT scanning (Micro CT Skyscan 1176, Bruker BioSpin, Belgium) for bone morphometric analysis. The scanning parameters included an isometric resolution of 20 mm and X-ray energy settings of 90 kV and 180 μA. All trabecular and cortical bone from each selected slice were segmented for 3D reconstruction to calculate bone mineral density (BMD, mg·cm^{-3}). The threshold was set from 52 to 255 for trabecular bone and from 50 to 255 for cortical bone. Scanning data were analyzed to determine the bone volume (BV, mm^3), bone volume/tissue volume (BV/TV, %), trabecular thickness (Tb. Th, μm), trabecular separation (Tb. Sp, μm) and trabecular number (Tb. N, 1/mm).

2.10. Hematoxylin and eosin (H&E) staining

Specimens extracted from the distal femurs underwent fixation and decalcification in a 15% ethylenediaminetetraacetic acid (EDTA) solution. The specimens were then dehydrated using a series of ethanol solutions of increasing concentration, followed by embedding in paraffin. Subsequently, 5 μm sections were cut parallel to the longitudinal axis of the bone and prepared for hematoxylin and eosin staining.

2.11. IHC analysis

Immunohistochemical staining was employed to analyze tissue sections for the presence of hypoxia and to quantify levels of hypoxyprobe-1, HIF-1α, VEGF, IL-6, ANGPTL4, and RANKL. Each antibody was applied according to the manufacturer's protocol. The number of positive cells was calculated per bone area (B. Ar), while the staining intensity was quantified using integrated optical density per area of positive cells (IOD/area, mean density). This analysis was conducted on six different images captured at 200 × magnification using Image-Pro Plus 6.0 software [20].

2.12. Methylthiazolyldiphenyl-tetrazolium (MTT)

MC3T3-E1 and MOB cells were seeded at a concentration of 4 × 10^4 cells/mL. The hypoxic groups were cultured in a hypoxic incubator (STEMCELL Technologies, Vancouver, Canada) with 1% O_2. CM collected from each group was mixed with osteoclast medium in a 1 : 3 ratio and incubated with osteoclasts for 48 h. After the 48 h incubation period, the medium was extracted, and 20 μL of 5 mg·mL^{-1} MTT solution was added to each well and incubated at 37 °C for 4 h. Subsequently, the medium was discarded, and 150 μL DMSO was added to the wells. The percentage of relative cell viability was determined using the formula: Relative cell viability = (experimental group/control) × 100%. Absorbance at 490 nm was measured using a microplate reader, and cell proliferation was calculated according to the following formula [21]:

$$\text{cell proliferation}\% = \frac{A_{\text{test group}} - A_{\text{blank group}}}{A_{\text{control group}} - A_{\text{blank group}}} \times 100\%$$

All experiments were performed in a minimum of three inde-

pendent replicates.

2.13. RNA isolation and real-time qPCR

The extraction of total RNA from cells was conducted using the TRIzol reagent according to the manufacturer's guidelines. Following RNA isolation, cDNA was synthesized using a cDNA Synthesis Kit. qPCR was performed using a Bio-Rad IQ5 (Bio-Rad) IQ5 system (Bio-Rad, USA) following the manufacturer's protocols for the setup procedure. The reaction mixture, with a total volume of 20 μL, included forward and reverse primers for the target genes *rankl*, *rank*, *trap*, *ctr*, *mmp-9* and catk as listed in Table 1. All experiments were conducted in triplicate. The relative expression level of each mRNA was normalized against β-actin and presented as fold change using the $2^{-\Delta\Delta Ct}$ method [22].

Table 1 Details of qPCR primer sequence

Gene	primer sequence (5'-3')
β-actin	F: 5'-GTGGACATCCGCAAAGAC-3'
	R: 5'-GCTGTCACCTTCACCGTTC-3'
rank	F: 5'-GCATCCCTTGCAGCTCAACA-3'
	R: 5'-ATGGAAGAGCTGCAGACCAC-3'
trap	F: 5'-TAACCGTCACCTGGCTGAAC-3'
	R: 5'-CACGGGACCCTAGTGCATTT-3'
ctr	F: 5'-TCACTGCTACATGTCACGCC-3'
	R: 5'-GTCACTGTCAAGGGTCCAGT-3'
mmp-9	F: 5'-CCAGCCGACTTTTGTGGTCT-3'
	R:5'-TGGCCTTTAGTGTCTGGCTG-3'
catk	F: 5'-CCGAAAAGAGCCTAGCGAAC-3'
	R: 5'-GGTCATGTCTCCCAAGTGGT-3'

2.14. ELISA

An ELISA was conducted to evaluate RANKL production in human osteoblastic cells. Initially, 1×10^5 cells were seeded in 24-well plates and incubated overnight. Subsequently, the cells were either maintained in a standard incubator, exposed to a hypoxic environment with 1% O_2, or treated with $CoCl_2$ for 24 hours. Following the treatment period, supernatants were collected and centrifuged for clarification. RANKL concentration was then determined using an ELISA kit according to the manufacturer's protocol. The ELISA experiments were performed in triplicate.

2.15. Western blot

The cells underwent lysis in RIPA lysis buffer for 30 min, and the resulting protein supernatant was quantified using a BCA kit. Proteins were separated by 10% SDS-PAGE gel and transferred onto polyvinylidene fluoride (PVDF) membranes at 4 ℃. Subsequently, the membranes were blocked with 5% BSA and incubated with primary antibodies, including Anti-HIF-1α (1 : 800) and Anti-β-actin (1 : 1500). The membranes were then developed using the EasyBlot ECL kit and analyzed with a multifunctional imager. The results were detected by a Tanon 5500 chemiluminescent imager system (Tanon Science & Technology; Shanghai, China) and standardized to β-actin protein. Western blotting experiments were conducted in triplicate.

2.16. Flow cytometry assay

The effect of SAL on osteoclast apoptosis was evaluated using an Annexin V-FITC/PI kit and flow cytometry. Cells were incubated with 100 μL of 1× Binding Buffer and 5 μL of Annexin V-FITC for 10 minutes in darkness. Subsequently, 10 μL of PI was added to the cells. Apoptosis was then analyzed using a flow cytometer. The flow cytometry assay was conducted with a minimum of three independent experiments to ensure reliability.

2.17. TRAP staining

The formation of osteoclasts was evaluated by exposing RAW264.7 and BMMs to CM derived from MC3T3-E1 and MOB for 6 days. Subsequently, TRAP staining was performed using a TRAP Stain Kit according to the manufacturer's instructions. Three random views were selected under microscopy (Olympus IX71, USA). TRAP-positive multinucleated cells (number of nuclei ≥ 3) were identified as osteoclasts. The quantity and spread area of multinucleated (number of nuclei ≥ 3) osteoclasts were measured under microscopy [23].

2.18. Bone resorption assay

For the bone resorption assay, bone slices were prepared and utilized. The slices were initially polished to a 100 μm thickness using a polishing machine and then cut into 5 mm × 5 mm pieces. These pieces were rinsed twice with PBS and ultrasonically cleaned for 10 mins. The sterilized bone slices were subsequently stored in DMEM containing 1% Penicillin-Streptomycin. The bone slices were then subjected to continuous SAL treatment. Both hypoxic and regular incubators were employed for cell incubation. In co-culture experiments, RAW264.7 and BMMs were stimulated with RANKL and M-CSF until osteoclast formation was observed. These cells were then seeded onto the treated bone slices and cultured with CM derived from MC3T3-E1 and MOB. After a 14-day incubation period, the bone slices were removed and stained with Toluidine Blue O solution. Following fixation, washing, dehydration, and staining, the bone lacunae were observed and measured *in vitro*. The percentage of resorption areas on the bone slices was analyzed using Image J software. The bone resorption experiment was conducted with a minimum of three independent repetitions.

2.19. Statistical analysis

Statistical analysis was performed using SPSS Statistics 21.0 software (IBM, USA). For comparisons between the two groups, t-tests were employed. One-way analysis of variance (ANOVA) was utilized to evaluate differences among three or more groups in normally distributed data. All data are presented as mean ± SD. GraphPad Prism 7 software (GraphPad Software) was used for graphing and further analysis. Statistical significance was denoted as $^*P < 0.05$.

3. Results

3.1. Hypoxia-induced RANKL upregulation correlates with HIF-1α overexpression

Initially, we examined the effect of hypoxia on RANKL expression in the MG-63 cell line. Exposing MG-63 cells to hypoxic conditions (1% O_2) or 0.5 mmol·L^{-1} $CoCl_2$ for 24 h resulted in a significant increase in RANKL mRNA and protein expression, as demonstrated by qPCR and ELISA analysis ($P < 0.05$) in Figs. 1A and B. YC-1 exhibited a notable inhibitory effect. Given its sensitivity to accumulation in hypoxic environments, the HIF-1α pathway is believed to play a crucial role in bone regeneration. Consequently, we hypothesized that the increase in RANKL expres-

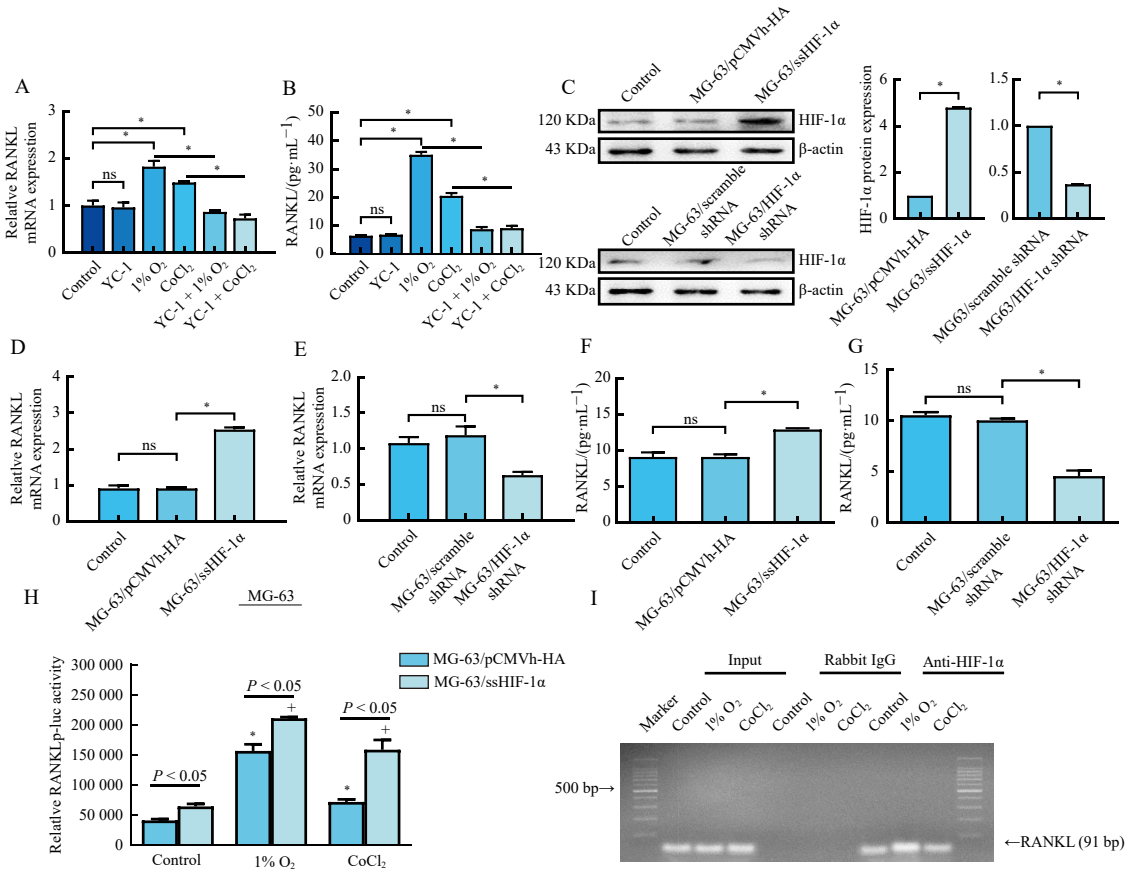

Fig. 1 Upregulation of RANKL induced by hypoxia was associated with overexpression of HIF-1α. (A, B) Hypoxia promoted the gene and protein expression of RANKL in MG-63 cells (n = 3). (C, D, F) The gene and protein expression of RANKL increased in MG-63/ssHIF-1α cells (n = 3). (C, E, G) The gene and protein expression of RANKL decreased in MG-63/shHIF-1α cells (n = 3). (H)Overexpression of HIF-1α mediated transcriptional activation of the RANKL promoter in MG-63 cells under hypoxia (n = 3). (I) Hypoxia promoted HIF-1α Binding to RANKL promoter (n = 3). The results are presented as the mean ± SD $^{*}P < 0.05$; $^{*}P < 0.05$.

sion was linked to active HIF-1α in osteoblastic cells. MG-63 cells were transfected with pCMVh-HA-ssHIF-1α (sense HIF-1α vector), HIF-1α shRNA, and the empty vector pCMVh-HA scramble shRNA using Lipofectamine™ 2000 for stable transfection. As shown in Figs. 1C, 1D and 1F, RANKL mRNA and protein expression significantly increased in MG-63/ssHIF-1α cells ($P < 0.05$). MG-63 cells demonstrated a marked decrease in RANKL expression after transient transfection with HIF-1α shRNA, as illustrated in Figs. 1C, 1E, and 1G ($P < 0.05$). These findings suggest that hypoxia induced the upregulation of HIF-1α, resulting in elevated RANKL levels in human osteoblasts.

3.2. Transcriptional regulation of RANKL under hypoxia is mediated via HIF-1α pathway

Next, we examined whether the enhanced regulation of RANKL occurred through transcriptional mechanisms. Human osteoblastic MG-63 cells were transfected with the pGL3-hRANKL promoter-luc and subsequently incubated in 1% O_2 or $CoCl_2$. As shown in Fig. 1H, HIF-1α overexpression increased the transcriptional activation of the RANKL promoter under hypoxic conditions in MG-63 cells. Furthermore, we investigated the binding activity of HIF-1α to RANKL promoters. MG-63 cells were incubated in 0.1% O_2 or treated with $CoCl_2$ for 24 h. Anti-HIF-1α antibodies and normal rabbit IgG were used for immunoprecipitation of sheared chromatin, followed by PCR amplification. Fig. 1I demonstrates that RANKL expression was significantly elevated in MG-63 cells under hypoxic conditions compared to normoxic conditions. This result indicates that HIF-1α binds to the promoter region of RANKL after nuclear translocation under hypoxia. These findings support our conclusion that HIF-1α can bind to the RANKL promoter, enhancing transcription in osteoblastic cells.

3.3. SAL prevents LPS-induced osteolytic bone loss in vivo

Animal experiments were conducted to investigate the potential anti-bone loss properties of SAL. LPS-induced deterioration in the microarchitecture of bone tissue was characterized by decreased thickness, lower density, diminished connectivity, and sparser trabeculae in the femur of mice (Fig. 2A). However, the administration of SAL at doses of 5 $mg·kg^{-1}$ and 20 $mg·kg^{-1}$ effectively inhibited the LPS-induced osteolysis. The SAL-treated groups demonstrated enhanced BV (mm^3), BV/TV (%), trabecular thickness (Tb. Th, μm), trabecular number (Tb. N, 1/mm), BMD (mg/cm^3), and reduced trabecular separation (Tb. Sp, μm) compared to the LPS group (Figs. 2B–2G). Histological assessment confirmed the preventive efficacy of SAL in mitigating LPS-induced osteolysis. Examination of H&E-stained histological sections revealed a higher degree of osteolysis in the LPS-induced group compared to the control group, while the SAL-treated LPS-induced group exhibited restoration of the bone matrix (Fig. 2H). Consistent with these findings, trabecular area (Tb.Ar, %), trabecular thickness (Tb. Th, μm), and trabecular number (Tb. N, 1/mm) were increased and trabecular separation (Tb. Sp, μm) was reduced in the SAL-treated groups when compared with the LPS group (Fig. 2I). TRAP staining showed that SAL reduced the number of TRAP-positive osteoclasts in the bone tissue (Figs. 2J and 2K). Moreover, immunohistochemical analysis revealed that SAL significantly alleviated bone tissue hypoxia and downregu-

lated the expression of HIF-1α, VEGF, IL-6, ANGPTL4, and RANKL. Additionally, SAL reduced the expression of Pimonidazole (hypoxyprobe-1) adducts, indicating decreased hypoxic areas in the bone tissue (Fig. 3). The results demonstrated that SAL significantly alleviated bone tissue hypoxia and downregulated the expression of HIF-1α while downregulating the expression of VEGF, IL-6, ANGPTL4 and RANKL, which were the downstream target genes of HIF-1α.

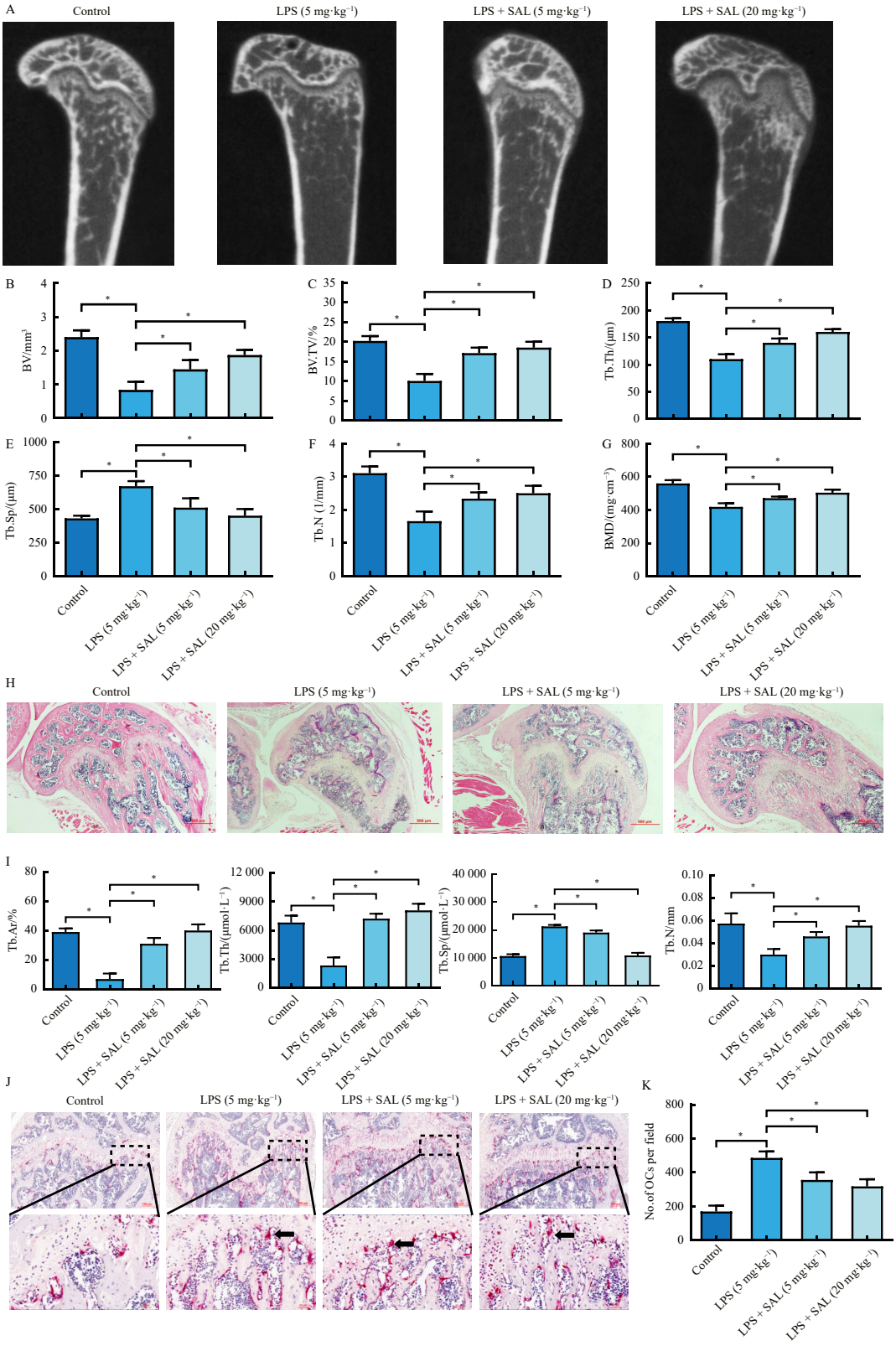

Fig. 2 SAL protects against LPS-induced bone loss in mice. (A)Representative images of micro-CT 3D microarchitecture of the femur (n = 8). (B–G) Scanning data were used to analyze bone volume (BV, mm^3), bone volume/tissue volume (BV/TV, %), trabecula thickness (Tb. Th, μm), trabecular separation (Tb. Sp, μm), trabecula number (Tb. N, 1/mm), bone mineral density (BMD, mg/cm^3) (n = 8). (H) H&E staining image. The scale bars represent 500 μm (n = 8). (I) The trabecular area (Tb.Ar, %), trabecula thickness (Tb. Th, μm), trabecular separation (Tb. Sp, μm), trabecula number (Tb. N, 1/mm) of bone sections (n = 8). (J–K) The number of TRAP-positive osteoclasts of tissue was analyzed using TRAP staining (n = 8). The scale bars represent 100 μm (n = 8). The results are presented as the mean ± SD. $^*P < 0.05$.

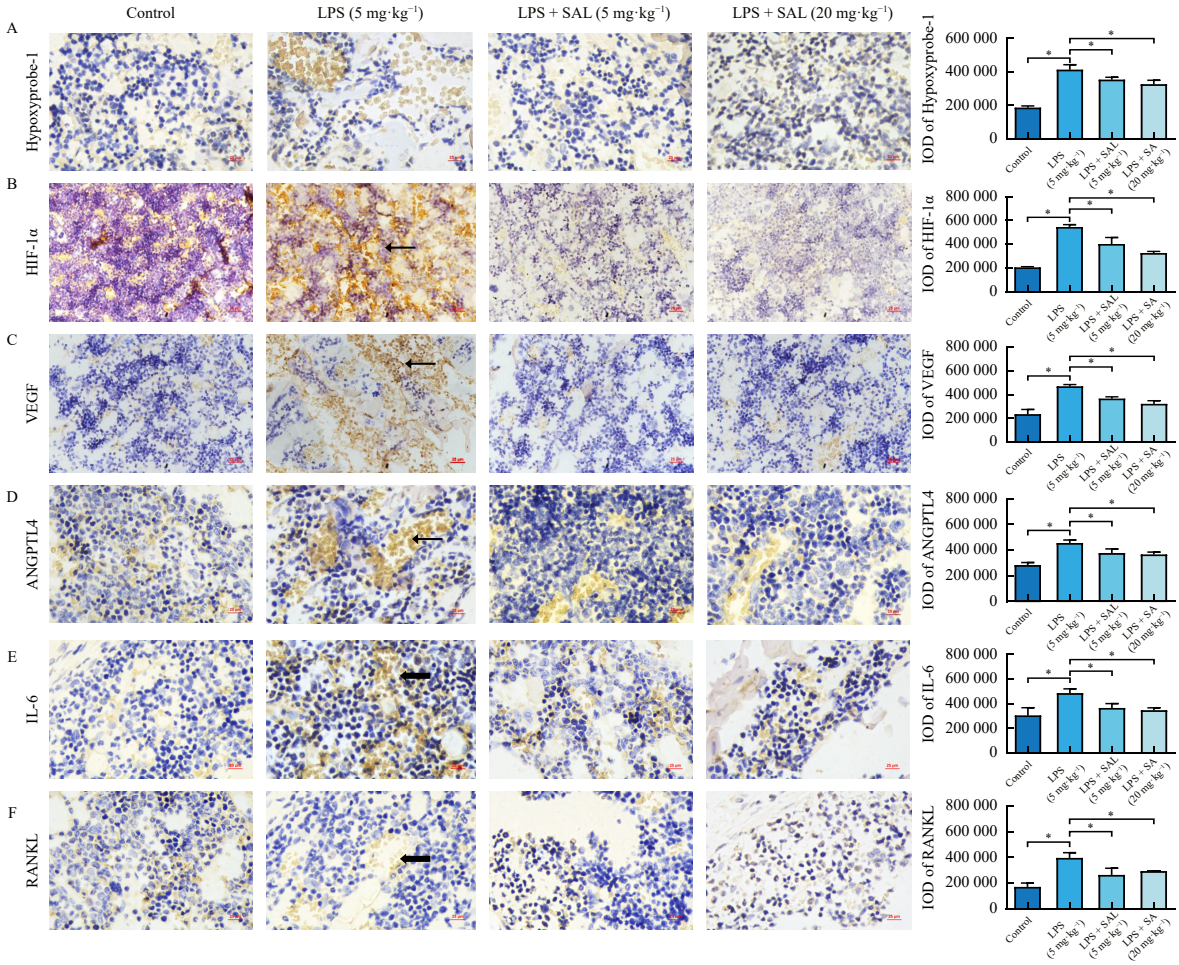

Fig. 3 SAL protects against LPS-induced bone loss in mice *via* HIF-1α/RANKL, VEGF, IL-6, and ANGPTL4 pathways. (A–F)The antibody of Pimonidazole (hypoxyprobe-1) adducts, HIF-1α, VEGF, IL-6, ANGPTL4, and RANKL were used to detect the expression of bone tissue hypoxia, HIF-1α, VEGF, IL-6, ANGPTL4, and RANKL by immunohistochemistry respectively (n = 8). The scale bars represent 25 μm. The results are presented as the mean ± SD. $^{*}P < 0.05$.

3.4. SAL inhibits osteoclastogenesis in a paracrine manner via HIF-1α pathway

The study indicates that SAL has the capacity to downregulate HIF-1α expression and its downstream target genes, thereby inhibiting osteolysis. This effect could potentially be attributed to SAL's role in modulating osteoblast and osteoclast activities. To explore whether SAL regulates the osteoblast-osteoclast interaction *via* the HIF-1α pathway, osteoblast culture supernatant was collected as CM. The MTT assay revealed that under hypoxic conditions, CM enhanced osteoclast cell viability. However, SAL treatment significantly reduced the cell viability of RAW264.7 and BMMs (Fig. 4A). Additionally, flow cytometric analysis showed that RAW264.7 cells treated with SAL for 48 h exhibited a notable increase in apoptotic rates (Fig. 4B). qPCR analysis results demonstrated a significant decrease in the gene expression of *Trap*, *ctr*, *rank*, *catk,* and *mmp-9* in both RAW264.7 and BMMs (Figs. 4C and 4D).

Based on these findings, this study further explored SAL's impact on osteoclast differentiation and bone resorption function through the activation of the osteoblast HIF-1α pathway. Observations revealed that osteoclasts in the 1%O_2 + CM group displayed an oval or irregular morphology with multiple nuclei. Following SAL administration, a significant reduction in the quantity of nuclei and TRAP-positive osteoclasts was observed. Consistent results were obtained from both RAW264.7 and BMMs (Figs. 5A and 5B). When RAW264.7 and BMMs were incubated with bovine cortical bone slices for 14 days, significant bone resorption lacunae were noted in the 1%O_2 + CM group, characterized by oval-shaped areas of increased volume. SAL diminished bone resorption, as evidenced by a reduction in the bone resorption area and pit number (Figs. 5C and 5D). However, the effects of SAL on osteoclasts through co-cultured osteoblasts were diminished to varying degrees after the addition of YC-1, Avastin, Anti-IL-6, MBL, and Denosumab. As the downstream of HIF-1α, SAL significantly inhibited osteoclast activity and the expression of differentiation genes through RANKL, VEGF, IL-6, and ANGPTL4 (Figs. 6A and 6B). It primarily inhibited osteoclast differentiation and bone resorption through the HIF-1α/VEGF and HIF-1α/RANKL pathways (Figs. 6C and 6D). Further investigation into the effect of combined blockade on SAL's action on osteoclasts revealed that combined blockade could completely reverse the SAL-mediated effect of HIF-1α (Fig. 7). Thus, the mechanistic study demonstrated that SAL regulated the phenotype of osteoclasts based on osteoblast-osteoclast interaction *via* the HIF-1α pathway.

4. Discussion

Microenvironmental hypoxia is a prevalent characteristic of osteolytic bone diseases, negatively impacting disease prognosis and progression. HIF-1, comprising HIF-1α and HIF-1β subunits, functions as a crucial transcriptional regulator in mediating cellular responses to hypoxia by interacting with the hypoxia-responsive element (HRE) and subsequently modulating target gene expression [24]. As a key regulator of hypoxia responses, HIF-1α significantly influences bone modeling, remodeling, and homeostasis processes [25]. RANKL, a type II transmembrane protein belonging

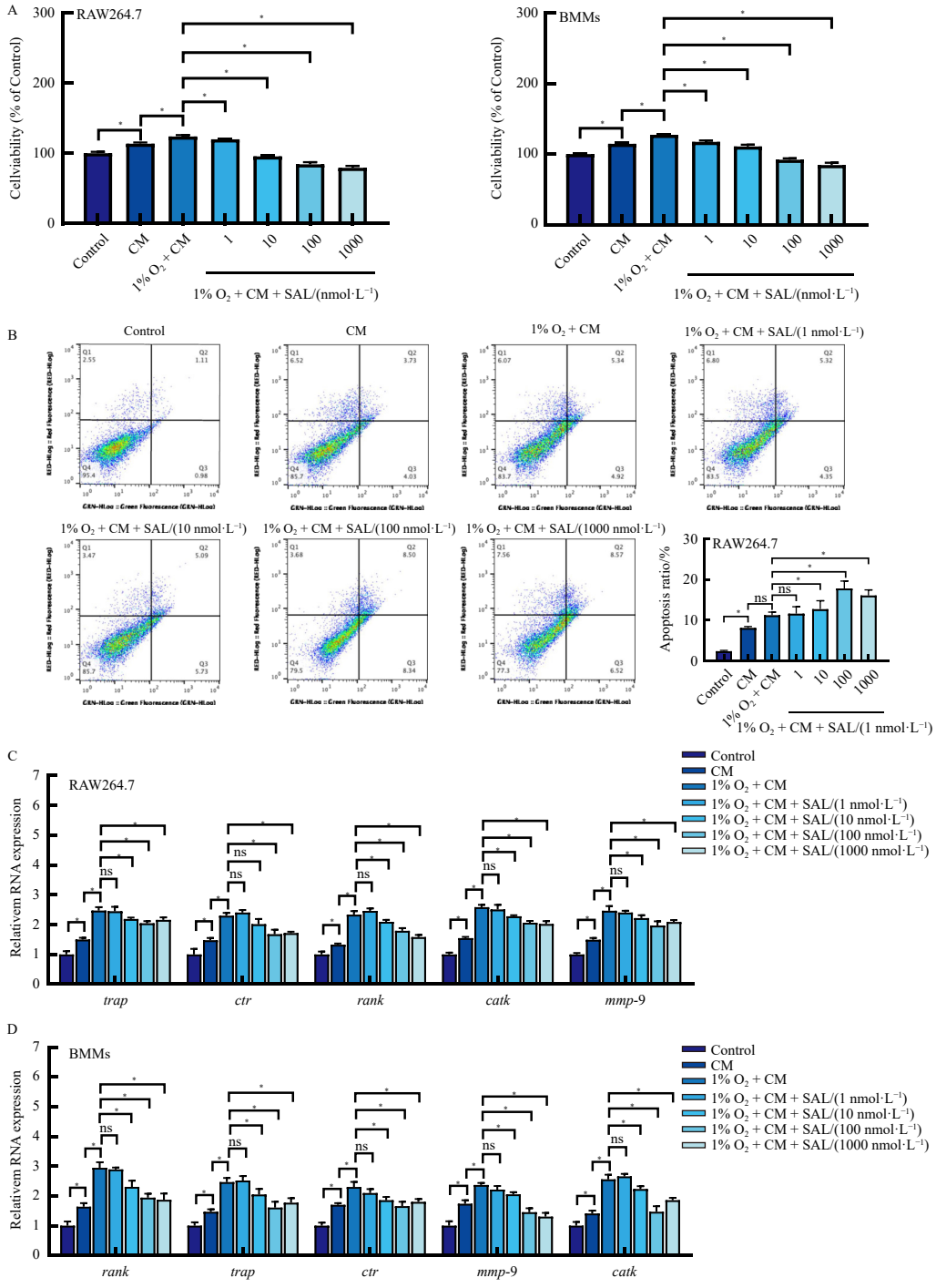

Fig. 4 The indirect effects of SAL on cell viability and differentiation-related genes expression of osteoclasts *via* hypoxic osteoblasts. (A)SAL inhibited cell viability of osteoclasts. (B)SAL enhanced apoptosis rate of RAW264.7 (n = 3). (C–D)SAL inhibited the gene expression of *trap*, *ctr*, *rank*, *catk* and *mmp-9* in osteoclasts (n = 3). The results are presented as the mean ± SD. $^{*}P < 0.05$.

to the tumor necrosis factor (TNF) superfamily [26], has been recognized as the primary modulator of mature osteoclast differentiation since its discovery as the principal determinant in osteoclast generation [27]. In this study, we demonstrated that activated HIF-1α signaling led to enhanced RANKL production and osteoclast formation. This result corroborates a previous study, which reported that deletion of HIF-1α prevented estrogen deficiency-induced bone loss in mice [28]. Additionally, our findings revealed that hypoxia-induced RANKL promoter activity increased notably with HIF-1α overexpression and enhanced RANKL promoter DNA binding ability under hypoxic conditions. These observations indicate that RANKL functions as a downstream target gene of HIF-1α in osteoblasts and plays a role in regulating osteoclast activity.

Rhodiola crenulata, a medicinal herb prevalent in high-altitude Tibetan regions, is renowned for enhancing tissue oxygenation, facilitating adaptation to high-altitude environments, and mitigating associated symptoms. SAL, the primary active compound in *Rhodiola crenulata*, exerts anti-hypoxia effects by scavenging reactive oxygen species, reducing calcium ion overload, and inhibiting apoptosis [29,30]. Additionally, SAL demonstrates pro-angiogenic effects through the HIF-1α-VEGF signaling pathway, contributing to the coordination of angiogenesis and osteogenesis is essential for bone health and repair [19]. ANGPTL4, a secreted

adipokine, independently promotes angiogenesis and is identified as a downstream target gene of HIF-1α, as revealed by DNA chip technology [14, 31]. Previous research has identified IL-6 as a downstream effector of HIF-1α, with its encoding gene being a newly discovered target of HIF-1α [32]. This study aimed to identify IL-6 as a downstream effector of HIF-1α, with its encoding gene being a newly discovered target of HIF-1α [32]. This study aimed to establish an LPS-induced osteolysis model and investigate the ef-

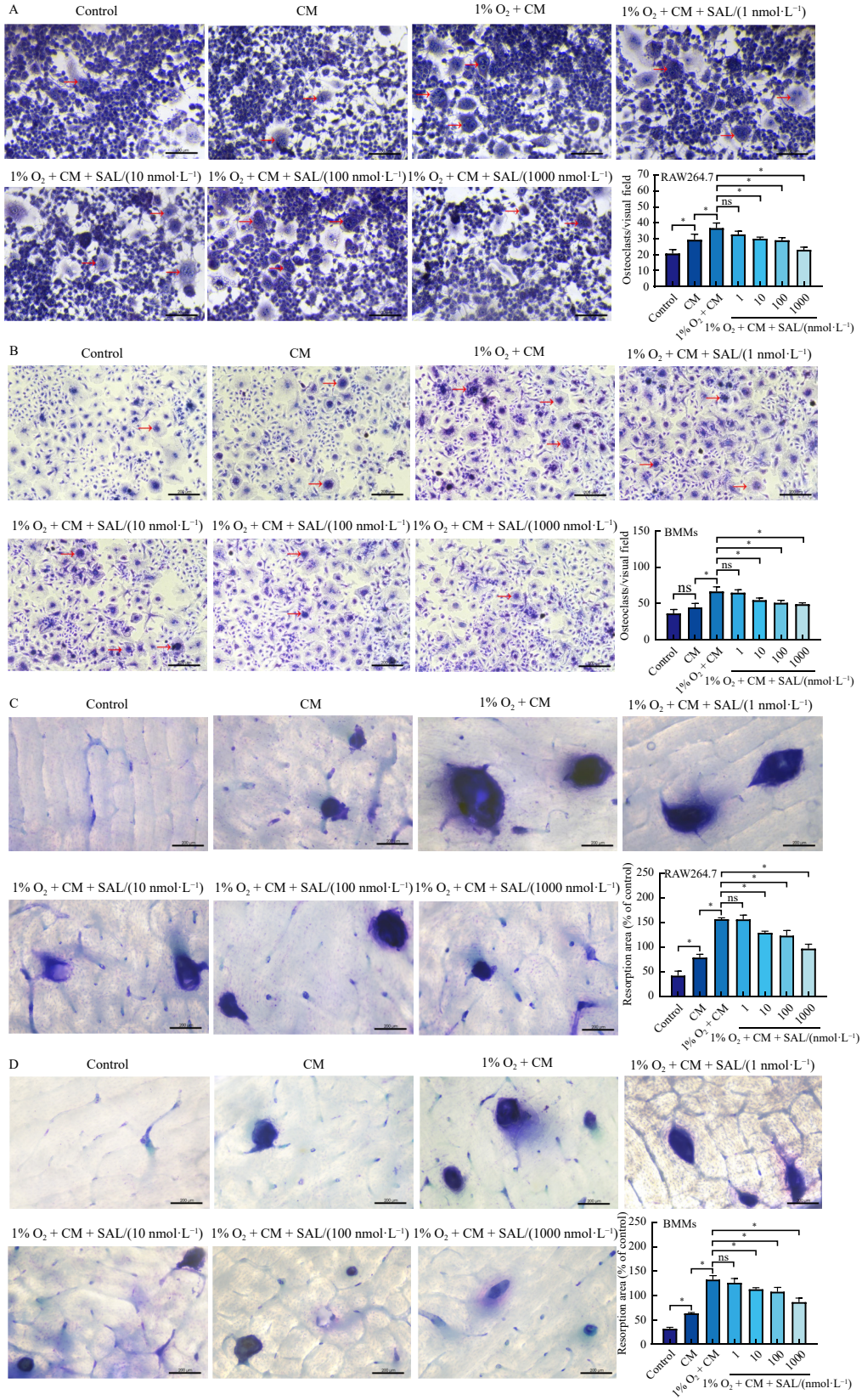

Fig. 5 The indirect effects of SAL on differentiation and bone resorption activity of osteoclasts via hypoxic osteoblasts. (A–B)SAL inhibited the number of multinucleated osteoclasts and TRAP activity of osteoclasts (n = 3). The scale bars represent 200 μm and 100 μm. (C–D)SAL inhibited bone resorption of osteoclasts (n = 3). The scale bars represent 200 μm. The results are presented as the mean ± SD. $^{*}P < 0.05$.

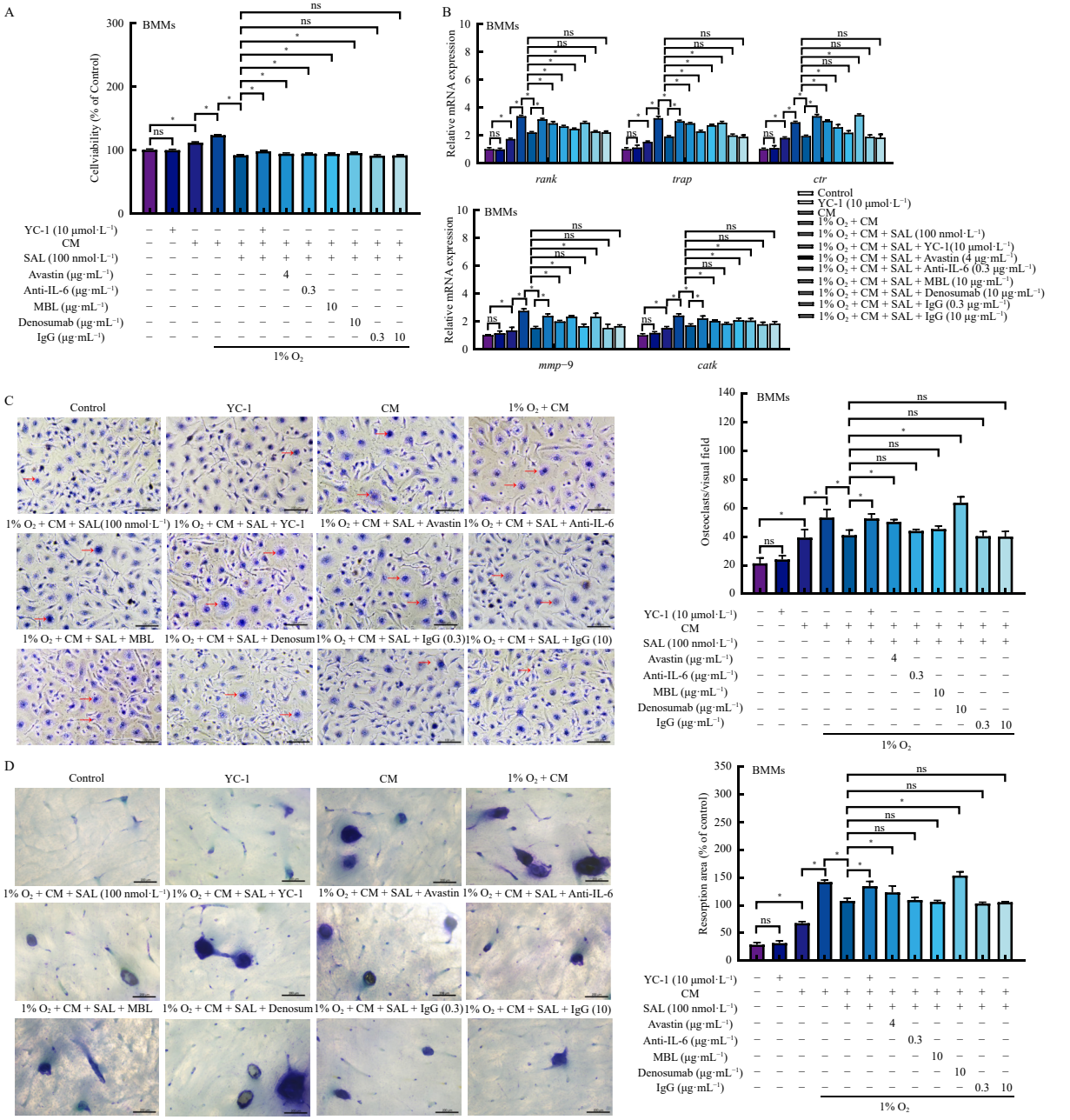

Fig. 6 The effects of the HIF-1α specific blocker YC-1 and neutralizing antibodies against VEGF, IL-6, and ANGPTL4 on osteoclasts via hypoxic osteoblasts. (A)The effect of SAL on the cell viability of osteoclasts was blocked with blocking antibodies (n = 3). (B)The effect of SAL on differentiation-related genes expression of osteoclasts were blocked with blocking antibodies (n = 3). (C)The effect of SAL on TRAP staining of osteoclasts was blocked with blocking antibodies. The scale bars represent 100 μm (n = 3). (D)The effect of SAL on bone resorption of osteoclasts was blocked with blocking antibodies (n = 3). The results are presented as the mean ± SD. $^{*}P < 0.05$.

fects of SAL intervention. SAL significantly alleviated bone tissue hypoxia and ameliorated bone loss in LPS-induced osteolysis by modulating the HIF-1α/RANKL axis and the expression of VEGF, IL-6, and ANGPTL4. As downstream target genes of HIF-1α expressed in osteoblasts, RANKL, VEGF, IL-6, and ANGPTL4 play crucial roles in regulating osteoclast differentiation and function. Subsequently, the study assessed the inhibitory effects of SAL on osteoclast activity.

The interplay between osteoblasts and osteoclasts is crucial in guiding the clinical management of osteolytic bone diseases. A comprehensive understanding of these cells' origin and function is essential for bone metabolism and the development of osteolytic disorders. Osteoblasts, originating from mesenchymal stem cells, are vital for bone formation. They possess the capacity to sense oxygen and detect changes in blood flow and oxygen pressure in bone tissue, particularly under hypoxic conditions on trabecular bone surfaces. Research has demonstrated the induction of HIF-1α expression in osteoblasts under hypoxia [33], and studies involving HIF-1α knockout mice have revealed a decrease in osteogenic capacity [34], emphasizing HIF-1α's critical role in osteoblast functionality and bone formation in low oxygen environments. In contrast, osteoclasts, multinucleated cells derived from monocytes, are responsible for bone resorption. Their differentiation is influenced by factors such as M-CSF and RANKL. The interaction between osteoblasts and osteoclasts is facilitated by the secretion of both paracrine and autocrine factors, with osteoblasts producing substances like M-CSF, RANKL, WNT5A, OPG, and WNT16 that regulate osteoclast formation and activity [35-37]. Based on these findings, we confirmed that SAL inhibited osteoclast differentiation through the HIF-1α pathway *via* osteoblast-osteoclast interactions. To evaluate the inhibitory effect of SAL on hypoxic osteoblasts through the paracrine pathway, we utilized various assays, including MTT, flow cytometry, qPCR, TRAP staining, and bone resorption assays. The results indicated that

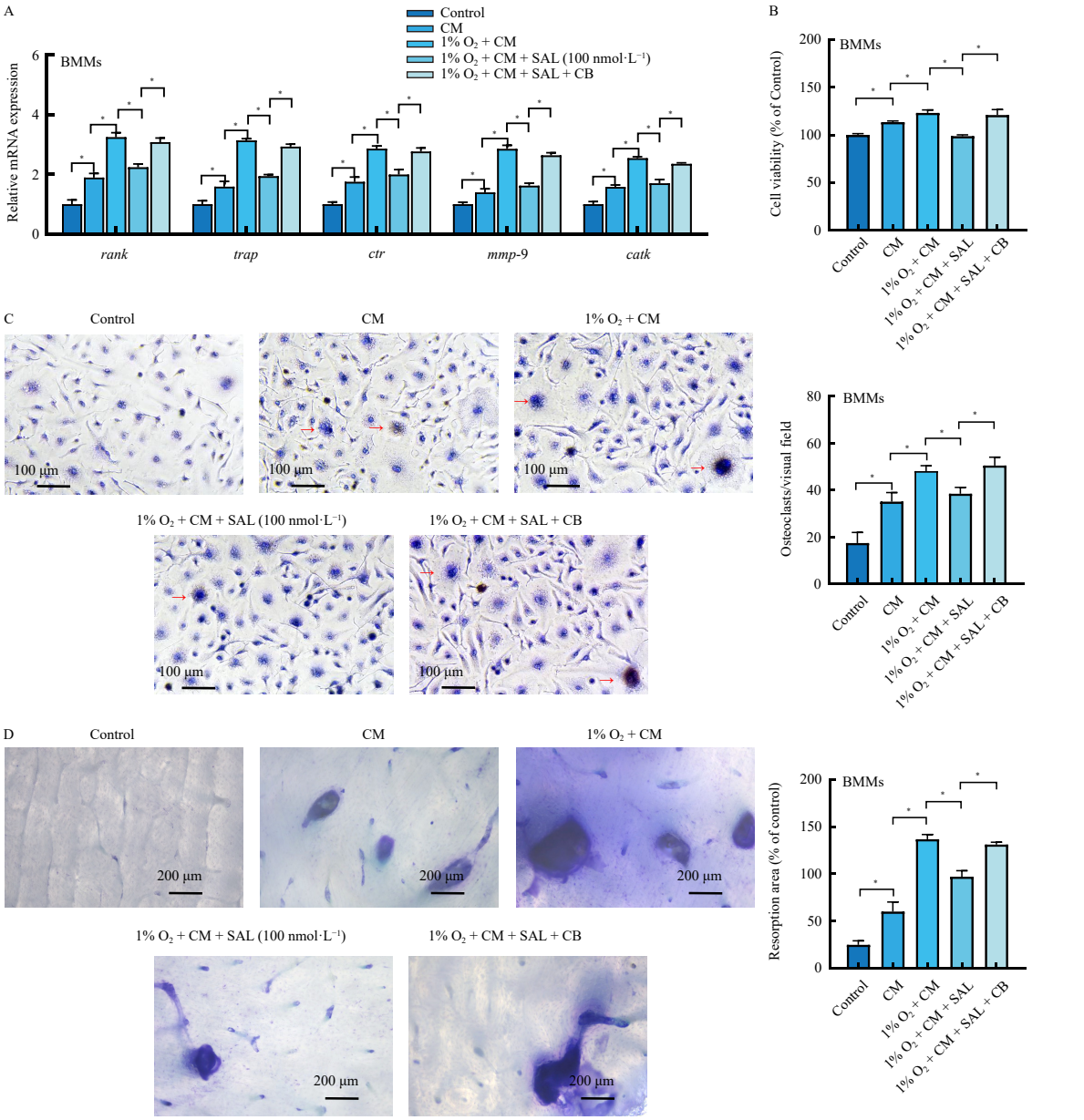

Fig. 7 The effects of the combined blockade on osteoclasts *via* hypoxic osteoblasts. (A)The effect of SAL on differentiation-related gene expression of osteoclasts was blocked with combinative blocking (n = 3). (B) The effect of SAL on the cell viability of osteoclasts was blocked with combinative blocking (n = 3). (C) The effect of SAL on TRAP staining of osteoclasts was blocked with combinative blocking (n = 3). The scale bars represent 100 μm. (D)The effect of SAL on bone resorption of osteoclasts was blocked with combinative blocking (n = 3). The scale bars represent 200 μm. The results are presented as the mean ± SD. $^{*}P < 0.05$.

the CM enhanced osteoclast viability, apoptosis, differentiation, and bone resorption activity, with these effects being more pronounced under hypoxic conditions. However, these effects were significantly mitigated in the hypoxia CM + SAL group. Moreover, the inhibitory effects were reversed upon the addition of specific blocking antibodies. Thus, SAL inhibited osteoclast differentiation and function under hypoxic conditions through pathways mediated by osteoblasts, involving HIF-1α/RANKL, VEGF, IL-6, and ANGPTL4 (Fig. 8).

LPS, a component of the outer membrane of Gram-negative bacteria, is a bacterial endotoxin that stimulates osteoclastogenesis by increasing the secretion of inflammatory cytokines and RANKL in an inflammatory environment. This process promotes the release of RANKL, which enhances osteoclast formation and osteolysis [38, 39]. Consequently, LPS is widely utilized in the study of inflammatory osteolysis [40-43]. The results of *in vivo* experiments demonstrate that SAL inhibited LPS-induced inflammatory bone loss in a dose-dependent manner. However, our experimental model was limited to LPS-induced local bone destruction of the femur in short-term experiments. Osteolytic diseases such as osteoporosis are typically long-term systemic conditions. Furthermore, multiple proinflammatory factors contribute to the development of osteolytic diseases. Therefore, additional *in vivo* studies, such as research on osteoporosis models induced by ovariectomy in mice, should be conducted to further elucidate the efficacy of SAL in treating osteoclast-related diseases.

Osteoclasts play a crucial role in bone resorption [44, 45], which is an essential process in the development of osteoporosis [46, 47] and other related bone disorders [48, 49]. SAL targets osteoblasts and inhibits osteoclast differentiation, potentially arresting the excessive bone resorption associated with these conditions. This intervention not only prevents further bone degradation but also aids in restoring bone density and strength. The mechanism of action of SAL provides a targeted therapeutic strategy to address

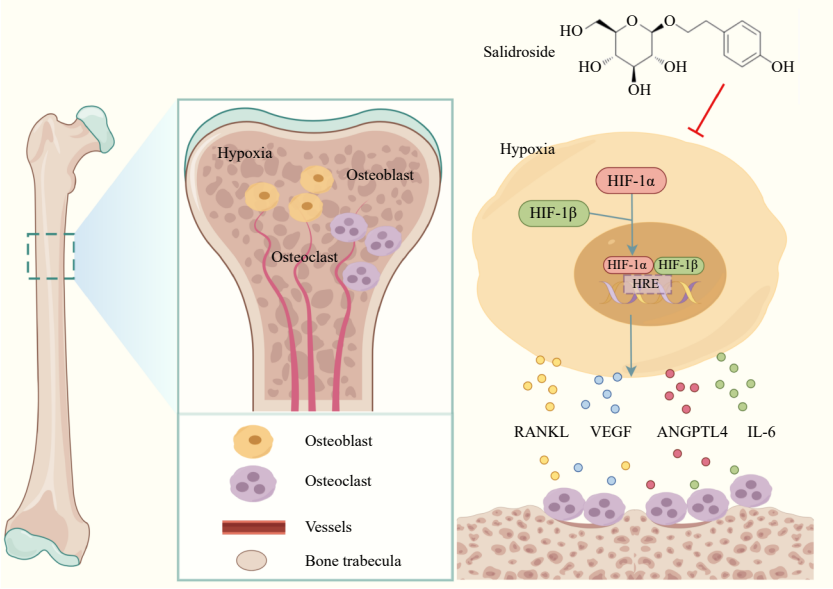

Fig. 8 Salidroside inhibits osteoclast differentiation through down-regulating HIF-1α/RANKL, VEGF, IL-6, and ANGPTL4 pathways based on osteoblast-osteoclast interaction (by Figdraw).

bone diseases by focusing on the fundamental cause of bone loss. This approach may lead to more effective osteoporosis treatments, potentially reducing fracture rates and improving the quality of life for patients with bone conditions.

5. Conclusion

Our findings substantiate that RANKL serves as a downstream target gene of HIF-1α in osteoblasts. SAL demonstrates significant efficacy in mitigating bone tissue hypoxia and attenuating bone loss in LPS-induced osteolysis through the HIF-1α/RANKL, VEGF, IL-6, and ANGPTL4 signaling pathways. Moreover, SAL exhibits inhibitory effects on osteoclast differentiation and function by modulating osteoblast paracrine secretion. These results underscore the therapeutic potential of SAL in preventing bone loss through the inhibition of osteoclastogenesis *via* the HIF-1α pathway.

Funding

This research was supported by grants from the National Natural Science Foundation of China (Nos. 81572852 and 82104671), the Great Program of the Science Foundation of Tianjin (No. 18JCZDJC33200), Heilongjiang Province Fund (No. LH2020H102), and Tianjin Key Medical Discipline (Specialty) Construction Project (No.TJYXZDXK-032A).

Ethics statement

All animal procedures were approved by the Ethics Committee of Tianjin University of Traditional Chinese Medicine （Approval No.: TCM-LAEC2020130）. The care, use, and treatment of mice adhered to the guidelines outlined in the Care and Use of Laboratory Animals.

Declaration of Competing Interest

These authors have no conflict of interest to declare.

References

1 Reid I R, Billington E O. Drug therapy for osteoporosis in older adults. *Lancet*. 2022;399(10329):1080-1092. https://doi.org/10.1016/S0140-6736(21)02646-5.
2 Jiajue R, Qi X, Jiang Y, et al. Incident fracture risk in type 2 diabetic postmenopausal women in mainland China: peking vertebral fracture study. *Calcif Tissue Int*. 2019;105(5):466-475. https://doi.org/10.1007/s00223-019-00598-x.
3 Fischer V, Haffner-Luntzer M. Interaction between bone and immune cells: implications for postmenopausal osteoporosis. *Semin Cell Dev Biol*. 2022;123:14-21. https://doi.org/10.1016/j.semcdb.2021.05.014.
4 Zeng Q, Li N, Wang Q, et al. The prevalence of osteoporosis in China, a nationwide, multicenter DXA Survey. *J Bone Miner Res*. 2019;34(10):1789-1797. https://doi.org/10.1002/jbmr.3757.
5 LeBoff MS, Greenspan SL, Insogna KL, et al. The clinician's guide to prevention and treatment of osteoporosis. *Osteoporos Int*. 2022;33(10):2049-2102. https://doi.org/10.1007/s00198-021-05900-y.
6 Ensrud KE. Bisphosphonates for postmenopausal osteoporosis. *JAMA*. 2021;325(1):96. https://doi.org/10.1001/jama.2020.2923.
7 Tao Z, Wang J, Wen K, et al. Pyroptosis in osteoblasts: a novel hypothesis underlying the pathogenesis of osteoporosis. *Front Endocrinol (Lausanne)*. 2020;11:548812.
8 Meng X, Wielockx B, Rauner M, et al. Hypoxia-inducible factors regulate osteoclasts in health and disease. *Front Cell Dev Biol*. 2021;9:658893. https://doi.org/10.3389/fcell.2021.658893.
9 Todd VM, Johnson RW. Hypoxia in bone metastasis and osteolysis. *Cancer Lett*. 2020;489:144-154. https://doi.org/10.1016/j.canlet.2020.06.004.
10 Stegen S, Carmeliet G. Hypoxia, hypoxia-inducible transcription factors and oxygen-sensing prolyl hydroxylases in bone development and homeostasis. *Curr Opin Nephrol Hypertens*. 2019;28(4):328-335. https://doi.org/10.1097/MNH.0000000000000508.
11 Tirpe AA, Gulei D, Ciortea SM, et al. Hypoxia: overview on hypoxia-mediated mechanisms with a focus on the role of HIF genes. *Int J Mol Sci*. 2019;20(24):6140. https://doi.org/10.3390/ijms20246140.
12 Lin C, McGough R, Aswad B, et al. Hypoxia induces HIF-1alpha and VEGF expression in chondrosarcoma cells and chondrocytes. *J Orthop Res*. 2004;22(6):1175-1181. https://doi.org/10.1016/j.orthres.2004.03.002.
13 Nguyen VT, Nardini M, Ruggiu A, et al. Platelet lysate induces in human osteoblasts resumption of cell proliferation and activation of pathways relevant for revascularization and regeneration of damaged bone. *Int J Mol Sci*. 2020;21(14):5123. https://doi.org/10.3390/ijms21145123.
14 Knowles HJ, Cleton-Jansen AM, Korsching E, et al. Hypoxia-inducible factor regulates osteoclast-mediated bone resorption: role of angiopoietin-like 4. *FASEB J*. 2010;24(12):4648-4659.
15 Niu X, Chen Y, Qi L, et al. Hypoxia regulates angeogenic-osteogenic coupling process *via* up-regulating IL-6 and IL-8 in human osteoblastic cells through hypoxia-inducible factor-1α pathway. *Cytokine*. 2019;113:117-127. https://doi.org/10.1016/j.cyto.2018.06.022.
16 Li W, Zhou X, Jiang T, et al. Positive effect of Gushukang on Type-H vessel and bone formation. *Front Cell Dev Biol*. 2020;8:265. https://doi.org/10.3389/fcell.2020.00265.
17 Yuan H, Xiao L, Min W, et al. Bu-Shen-Tong-Luo Decoction prevents bone loss *via* inhibition of bone resorption and enhancement of angiogenesis in ovariectomy-induced osteoporosis of rats. *J Ethnopharmacol*. 2018;220:228-238. https://doi.org/10.1016/j.jep.2018.01.007.
18 Wang YF, Chang YY, Zhang XM, et al. Salidroside protects against osteoporosis in ovariectomized rats by inhibiting oxidative stress and promoting osteogenesis *via* Nrf2 activation. *Phytomedicine*. 2022;99:154020. https://doi.org/10.1016/j.phymed.2022.154020.
19 Guo Q, Yang J, Chen Y, et al. Salidroside improves angiogenesis-osteogenesis coupling by regulating the HIF-1α/VEGF signalling pathway in the bone environment. *Eur J Pharmacol*. 2020;884:173394. https://doi.org/10.1016/j.

ejphar.2020.173394.
20 Liu W, Wang Z, Yang J, et al. Osteocyte TSC1 promotes sclerostin secretion to restrain osteogenesis in mice. *Open Biol*. 2019;9(5):180262. https://doi.org/10.1098/rsob.180262.
21 Xu M, Sun S, Ge J, et al. Bupleurum chinense polysaccharide improves LPS-induced senescence of RAW264.7 cells by regulating the NF-κB signaling pathway. *Evid Based Complement Alternat Med*. 2020;2020:7060812.
22 Sharma Y, Ahmad A, Yavvari PS, et al. Targeted SHP-1 silencing modulates the macrophage phenotype, leading to metabolic improvement in dietary obese mice. *Mol Ther Nucleic Acids*. 2019;16:626-636. https://doi.org/10.1016/j.omtn.2019.04.020.
23 Qiu Z, Li L, Huang Y, et al. Puerarin specifically disrupts osteoclast activation via blocking integrin-β3 Pyk2/Src/Cbl signaling pathway. *J Orthop Translat*. 2022;33:55-69. https://doi.org/10.1016/j.jot.2022.01.003.
24 Masoud GN, Li W. HIF-1α pathway: role, regulation and intervention for cancer therapy. *Acta Pharm Sin B*. 2015;5(5):378-389. https://doi.org/10.1016/j.apsb.2015.05.007.
25 Chen W, Wu P, Yu F, et al. HIF-1α regulates bone homeostasis and angiogenesis, participating in the occurrence of bone metabolic diseases. *Cells*. 2022;11(22):3552. https://doi.org/10.3390/cells11223552.
26 Ono T, Hayashi M, Sasaki F, et al. RANKL biology: bone metabolism, the immune system, and beyond. *Inflamm Regen*. 2020;40:2. https://doi.org/10.1186/s41232-019-0111-3.
27 McDonald MM, Khoo WH, Ng PY, et al. Osteoclasts recycle *via* osteomorphs during RANKL-stimulated bone resorption. *Cell*. 2021;184(5):1330-1347. https://doi.org/10.1016/j.cell.2021.02.002.
28 Meng X, Lin Z, Cao S, et al. Estrogen-mediated downregulation of HIF-1α signaling in B lymphocytes influences postmenopausal bone loss. *Bone Res*. 2022;10(1):15. https://doi.org/10.1038/s41413-022-00189-x.
29 Wu Y, Ma Y, Li J, et al. The bioinformatics and metabolomics research on anti-hypoxic molecular mechanisms of Salidroside *via* regulating the PTEN mediated PI3K/Akt/NF-κB signaling pathway. *Chin J Nat Med*. 2021;19(6):442-453.
30 Xiong Y, Wang Y, Xiong Y, et al. Protective effect of Salidroside on hypoxia-related liver oxidative stress and inflammation *via* Nrf2 and JAK2/STAT3 signaling pathways. *Food Sci Nutr*. 2021;9(9):5060-5069. https://doi.org/10.1002/fsn3.2459.
31 Costa-Rodrigues J, Fernandes A, Fernandes MH. Reciprocal osteoblastic and osteoclastic modulation in co-cultured MG63 osteosarcoma cells and human osteoclast precursors. *J Cell Biochem*. 2011;112(12):3704-3713. https://doi.org/10.1002/jcb.23295.
32 Crockett JC, Mellis DJ, Scott DI, et al. New knowledge on critical osteoclast formation and activation pathways from study of rare genetic diseases of osteoclasts: focus on the RANK/RANKL axis. *Osteoporos Int*. 2011;22(1):1-20. https://doi.org/10.1007/s00198-010-1272-8.
33 Wang Y, Wan C, Deng L, et al. The hypoxia-inducible factor alpha pathway couples angiogenesis to osteogenesis during skeletal development. *J Clin Invest*. 2007;117(6):1616-1626. https://doi.org/10.1172/JCI31581.
34 Udagawa N, Koide M, Nakamura M, et al. Osteoclast differentiation by RANKL and OPG signaling pathways. *J Bone Miner Metab*. 2021;39(1):19-26. https://doi.org/10.1007/s00774-020-01162-6.
35 Han Y, You X, Xing W, et al. Paracrine and endocrine actions of bone-the functions of secretory proteins from osteoblasts, osteocytes, and osteoclasts. *Bone Res*. 2018;6:16. https://doi.org/10.1038/s41413-018-0019-6.
36 Lotinun S, Kiviranta R, Matsubara T, et al. Osteoclast-specific cathepsin K deletion stimulates S1P-dependent bone formation. *J Clin Invest*. 2013;123(2):666-681.
37 Maeda K, Kobayashi Y, Udagawa N, et al. Wnt5a-Ror2 signaling between osteoblast-lineage cells and osteoclast precursors enhances osteoclastogenesis. *Nat Med*. 2012;18(3):405-412. https://doi.org/10.1038/nm.2653.
38 Wang H, Cao X, Guo J, et al. BNTA alleviates inflammatory osteolysis by the SOD mediated anti-oxidation and anti-inflammation effect on inhibiting osteoclastogenesis. *Front Pharmacol*. 2022;13:939929. https://doi.org/10.3389/fphar.2022.939929.
39 Song C, Yang X, Lei Y, et al. Evaluation of efficacy on RANKL induced osteoclast from RAW264.7 cells. *J Cell Physiol*. 2019;234(7):11969-11975. https://doi.org/10.1002/jcp.27852.
40 Wu X, Zhao K, Fang X, et al. Inhibition of lipopolysaccharide-induced inflammatory bone loss by Saikosaponin D is associated with regulation of the RANKL/RANK pathway. *Drug Des Devel Ther*. 2021;15:4741-4757. https://doi.org/10.2147/DDDT.S334421.
41 Sharma K, Kumar S, Prakash R, et al. Chebulinic acid alleviates LPS-induced inflammatory bone loss by targeting the crosstalk between reactive oxygen species/NFκB signaling in osteoblast cells. *Free Radic Biol Med*. 2023;194:99-113. https://doi.org/10.1016/j.freeradbiomed.2022.11.026.
42 Hu J, Li X, Chen Y, et al. The protective effect of WKYMVm peptide on inflammatory osteolysis through regulating NF-κB and CD9/gp130/STAT3 signalling pathway. *J Cell Mol Med*. 2020;24(2):1893-1905. https://doi.org/10.1111/jcmm.14885.
43 Park HJ, Gholam ZM, Suh JH, et al. Dauricine protects from LPS-induced bone loss *via* the ROS/PP2A/NF-κB axis in osteoclasts. *Antioxidants (Basel)*. 2020;9(7):588. https://doi.org/10.3390/antiox9070588.
44 Bordukalo-Nikšić T, Kufner V, Vukičević S. The role of BMPs in the regulation of osteoclasts resorption and bone remodeling: from experimental models to clinical applications. *Front Immunol*. 2022;13:869422. https://doi.org/10.3389/fimmu.2022.869422.
45 Veis D J, O'Brien C A. Osteoclasts, master sculptors of bone. *Annu Rev Pathol*. 2023;18:257-281. https://doi.org/10.1146/annurev-pathmechdis-031521-040919.
46 Da W, Tao L, Zhu Y. The role of osteoclast energy metabolism in the occurrence and development of osteoporosis. *Front Endocrinol (Lausanne)*. 2021;12:675385. https://doi.org/10.3389/fendo.2021.675385.
47 Tao H, Li W, Zhang W, et al. Urolithin A suppresses RANKL-induced osteoclastogenesis and postmenopausal osteoporosis by, suppresses inflammation and downstream NF-κB activated pyroptosis pathways. *Pharmacol Res*. 2021;174:105967. https://doi.org/10.1016/j.phrs.2021.105967.
48 Andreev D, Liu M, Weidner D, et al. Osteocyte necrosis triggers osteoclast-mediated bone loss through macrophage-inducible C-type lectin. *J Clin Invest*. 2020;130(9):4811-4830. https://doi.org/10.1172/JCI134214.
49 Agidigbi T S, Kim C. Reactive oxygen species in osteoclast differentiation and possible pharmaceutical targets of ROS-mediated osteoclast diseases. *Int J Mol Sci*. 2019;20(14):3576. https://doi.org/10.3390/ijms20143576.